MICROSTRUCTURE MODIFICATIONS OF Al-Si-COATED PRESS-HARDENED STEEL 22MnB5 BY LASER WELDING

[1]Hana ŠEBESTOVÁ, [1]Petr HORNÍK, [1]Filip MIKA, [1]Šárka MIKMEKOVÁ, [1]Ondřej AMBROŽ, [1]Libor MRŇA

[1]Institute of Scientific Instruments of the Czech Academy of Sciences, Brno, Czech Republic, EU,
sebestova@isibrno.cz, hornik@isibrno.cz, fumici@isibrno.cz, sarka@isibrno.cz, ondrej@isibrno.cz, mrna@isibrno.cz

https://doi.org/10.37904/metal.2023.4646

Abstract

Weld microstructure depends on the characteristics of welded materials and parameters of welding technology, especially on the heat input that determines the peak temperature and the cooling rate. When the coated sheets are welded, the effect of the chemical composition of the coating must be also considered even though its thickness is only a few tens of microns. During 22MnB5+AlSi laser welding experiments, the ferrite-stabilizing elements of coating modified the weld metal microstructure. Ferrite appeared in a quenched weld metal. The rapid cooling rate accompanying welding with a focused beam limited the homogenization of the weld metal which resulted in the formation of ferritic bands in the regions rich in Si and especially in Al. On the other hand, a high level of homogenization was reached when welding with the defocused beam. The ferritic islands uniformly distributed in the weld metal were formed at 0.4 wt% and 1.6 wt% of Si and Al, respectively. The doubled heat input reduced the Al content to 0.7 wt% insufficient for the ferrite formation at still relatively high cooling rates. Predicting the distribution of ferrite in the weld metal is challenging due to its dependence on various factors, such as cooling rate and the volume of dissolved coating, which may vary with any modifications made to the welding parameters.

Keywords: Laser welding, high-strength steel, microstructure, heat input, ferrite stabilization

1. INTRODUCTION

The microstructure of normalized press-hardenable steel 22MnB5 is ferritic-pearlitic. During the hot-stamping process, it is quenched in a cooled die to reach high tensile and fatigue strength [1]. The stamped parts are further assembled and joined to other components of a final construction, typically a car body. Laser welding is a suitable method of joining thin sheets thanks to its highly concentrated energy minimizing the heat input and thus the distortions. Rapid cooling rate, characteristic of laser welding, produces quenched microstructure of weld metal maintaining high strength. The inter-critical heat-affected zone with reduced microhardness is supposed to be the weakest link of the 22MnB5 laser weld joint [2, 3]. However, the steel sheets are usually coated with Al-Si to prevent surface oxidation during the austenitization preceding the forming [4]. If the coating is not removed before welding, it can have a negative effect on the strength of the weld metal [5-7].

In laser welding, the high demands on sheet edges preparation, precise fit-up, and beam positioning must be fulfilled because a laser beam is typically only a few tens of millimeters in diameter. A defocused beam of higher power can be used to circumvent these demands. Similarly, laser welding with beam oscillation was introduced to increase the gap-bridging ability of the beam and the stability of the process [8, 9]. In our research, we investigate both approaches and explain the resulting consequences on the formation of weld metal microstructure. This paper aims to demonstrate that any modification in welding technology or its parameters can have a significant impact on the microstructure of the weld metal of coated sheets.

2. EXPERIMENT

The IPG fiber laser YLS-2000 with a maximum output power of 2 kW was used for 22MnB5 (trade name Usibor 1500) bead-on-plate welding experiments. The 1.5 mm thin sheets with Al-Si coating 150 g·m^{-2} were in hot-stamped condition. The optical fiber with a diameter of 100 μm delivered the laser beam into the IPG wobbling head FLW-D30-W mounted on the arm of the ABB robot IRB 2400. The sheets were welded with both a focused beam, a defocused beam, and an oscillating focused beam. The beam focused on the sheet surface and the defocused beam reached the spot diameter of 0.2 mm and 3 mm, respectively. The welding was carried out in a protective argon atmosphere. Subsequently, the same set of experiments was repeated with sheets with mechanically removed Al-Si coating to evaluate the effect of coating at various processing parameters. Samples with removed coating are assigned with "R". Welding parameters with sample designation are summarized in **Table 1**. Here, the heat input is defined as a portion of laser power and welding speed. For the sake of simplicity, we assume a 100% absorption efficiency.

Table 1 Welding parameters

Weld no.		**Welding speed (mm·s^{-1})**	**Laser power (W)**	**Heat input (J·mm^{-1})**	**Spot diameter (mm)**	**Oscillation diameter; frequency (mm; Hz)**
with coating	removed coating					
1	1R	20	1,300	65	0.2	-
2	2R	20	2,000	100	3.0	-
3	3R	10	2,000	200	3.0	-
4	4R	20	1,300	65	0.2	4; 100

An unconventional oscillation mode "atom" was used for weld 4. The velocity of the laser spot moving along the static trajectory of oscillation mode sums with the vector of the welding speed [10], and the spot trajectory (moving trajectory) is created (**Figure 1**). The speed of the spot continuously changes along the trajectory of the oscillation mode.

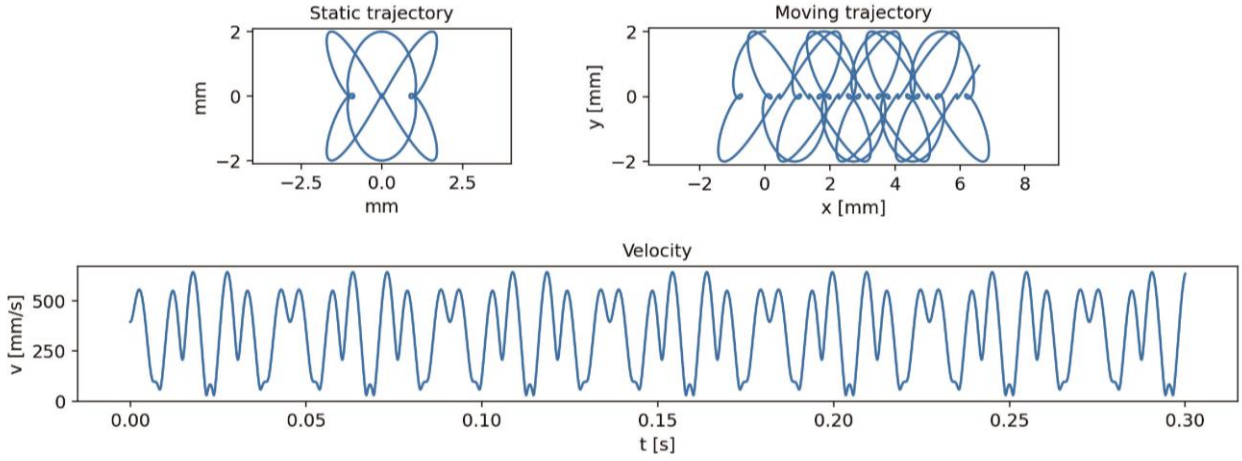

Figure 1 Static oscillation mode "atom", spot trajectory, and fluctuations of spot speed on the material surface

3. EXPERIMENTAL RESULTS AND DISCUSSION

The welds were cut perpendicularly to the welding direction and metallographic specimens of weld cross-sections were prepared. The specimens were etched with 4% nital for 3 s to reveal the microstructure. Similarly, the metallographic specimens of weld surfaces were prepared. The macro- and microstructure of

weld metal were observed with Keyence laser scanning confocal microscope VK-X Series 3D. The FEI scanning electron microscope MAGELLAN 400 with the AMETEK EDAX Octane Elect Super Silicon Drift Detector and EDAX Hikari were used for EDS and EBSD, respectively. The EDS analysis of areas 3 μm × 3 μm was performed at 20 keV landing energy of the primary electrons and beam current of 3.2 nA. The EBSD data were collected at th same conditions with the step size of 50 nm.

3.1 Weld macrostructure

The weld surfaces were documented to demonstrate the effect of Al-Si coating presence (**Figure 2**). The white-etched macroscopic formations were found in the weld metal of coated sheets. Their size and distribution differ for each sample. The largest white-etched curved bands are in weld 4 made with beam oscillation. Much smaller islands of white-etched phase relatively homogeneously distributed throughout the weld metal are present in weld 2 made with the defocused beam. Finally, only a few random bands close to the fusion line and small-sized islands underneath the surface were found in welds 1 and 3, respectively. The welds of de-coated sheets are free of these formations.

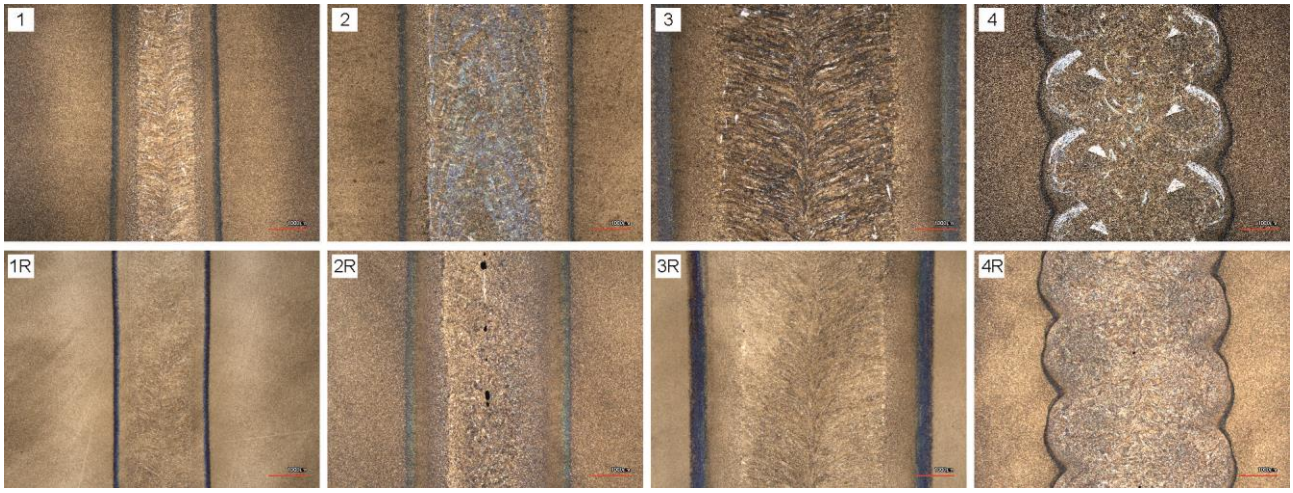

Figure 2 Macrostructure of weld surface of coated (1 - 4) and de-coated sheets (1R - 4R), scale 1 mm

Different weld widths of corresponding welds in **Figure 2** result from the metallographic preparation. The volume of the material removed during the grinding was not constant for all specimens. Cross-section specimens must be used for the weld shape assessment. The shape of a weld is almost independent of the Al-Si coating presence. Therefore, only welds 1 - 4 (sheets with the coating) are shown in **Figure 3**. The weld 1 made with the focused beam is of an hourglass shape, narrow, and fully penetrated. The welds made with the defocused beam do not reach the full penetration, even the maximal laser power and the half welding speed was used to triple the heat input. The low power density of the beam led to the conduction mode welding characterized by a low aspect (depth-to-width) ratio. It reached 0.2 and 0.3 for welds 2 and 3, respectively. The width measured on the sheet surface of welds 3 and 4 is comparable. However, weld 4 reached full penetration with a narrow root. The large, curved bands of white-etched phase are visible on the weld 4 cross-sections, especially on weld peripheries, where the spot speed reaches the highest values.

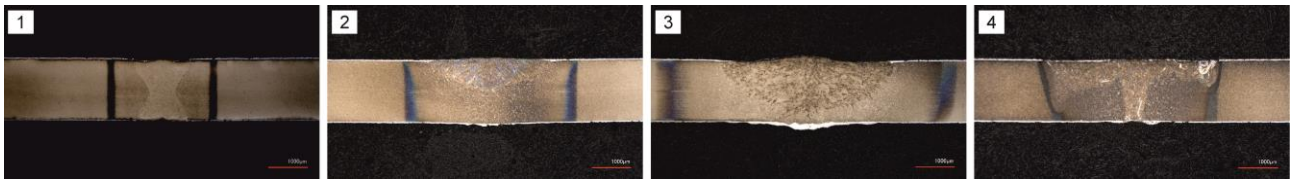

Figure 3 Macrostructure of weld cross-section of coated sheets 1 - 4, scale 1 mm

Weld dimensions of coated sheets and a portion of the area of coating towards the area of weld metal (coating content) in weld cross-sections are summarized in **Table 2**. The area of the coating was calculated as a product of the weld width and thickness of the coating that reached (40 ± 2) μm (measured with PosiTector 6000). Weld 2 has the highest coating content which corresponds to the poorest aspect ratio.

Table 2 Weld dimensions of coated sheets

Sample	Weld metal				Weld metal + heat affected zone	
	Width (mm)	Depth (mm)	Area (mm^2)	Coating content (%)	Width (mm)	Area (mm^2)
1	1.5	1.5	1.1	7	2.8	4.2
2	3.2	0.8	1.6	8	4.3	7.0
3	4.4	1.3	4.4	4	7.6	11.8
4	4.4	1.5	3.1	6	4.7	6.8

3.2 Weld metal microstructure

The microstructure of HAZ of 22MnB5 laser welds was described in detail in our previous paper [7]. We do not expect any significant effect of the coating presence on the HAZ microstructure. Therefore, only the microstructure of weld metal is analyzed in this chapter. **Figure 4** presents the comparison of the microstructure of weld metal along the weld axis in the middle of the weld depth.

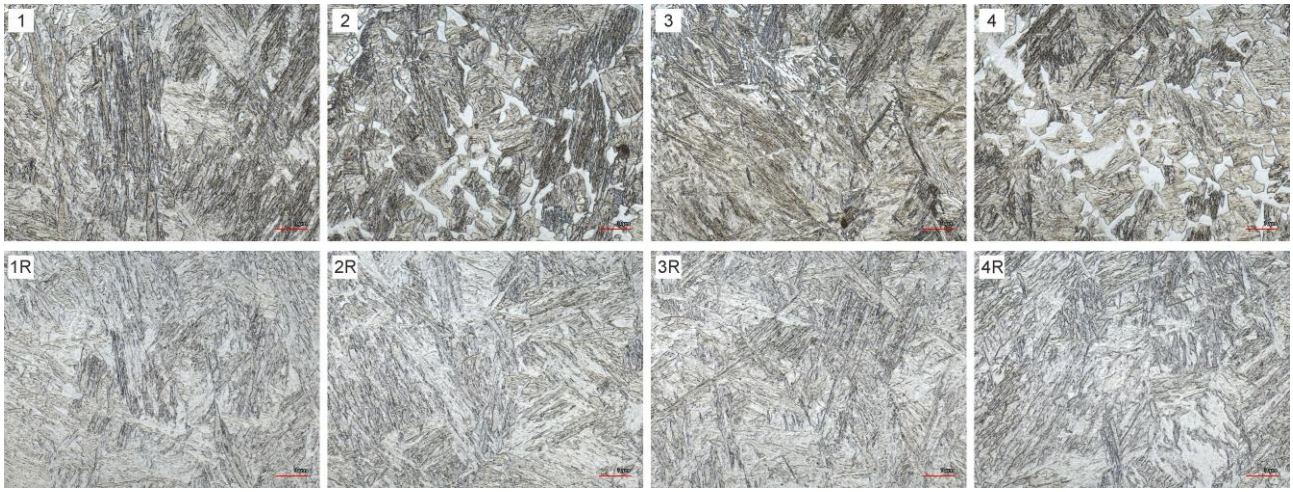

Figure 4 Microstructure of the weld metal of coated (1 - 4) and de-coated sheets (1R - 4R), scale 10 μm

The EBSD measurement discovered the body-centered cubic crystal lattice for both the matrix and the white-etched phase (**Figure 5**). Based on the image quality map, the white-etched phase was identified as a ferrite interspersed in a quenched matrix. The matrix was supposed to be martensitic. However, more than one half of the boundaries are high-angel (> 15°) in the weld 4R which indicates rather a bainitic-martensitic matrix.

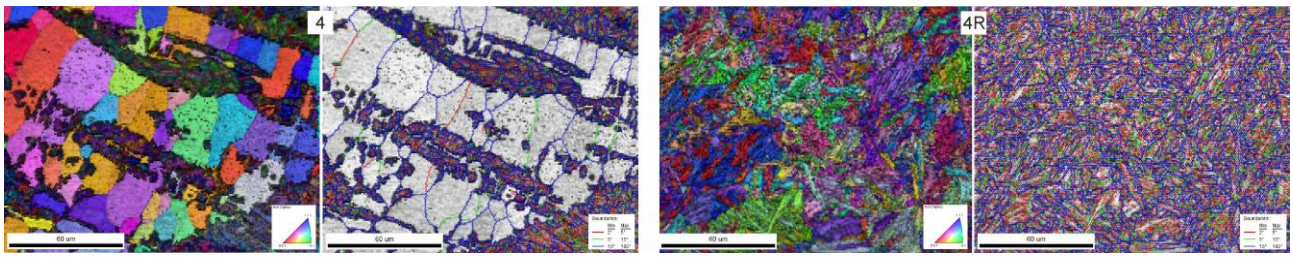

Figure 5 The inverse pole figure map and the boundaries map of weld metal of weld 4 and 4R, scale 60 μm

The EDS analysis of weld cross-sections revealed the increase in the portion of Si and Al in the weld metal of coated sheets towards the base metal. The weld metal matrix consists of (0.3 - 0.5) wt% and (0.7 - 2) wt% of Si and Al, respectively. The highest contents were detected between the large bands of ferrite in weld 4 close to the weld surface. The minimal increase was in weld 3 which is almost free of ferritic islands (**Figure 6**). Excluding weld 4, the differences measured within the one weld were comparable to the average measurement errors of 0.05 wt% and 0.2 wt% for Si and Al, respectively. Similarly, concerning the measurement errors, the difference between the content of monitored elements in the ferrite and surrounding matrix was negligible. Therefore, **Table 3** presents the average matrix data for each weld.

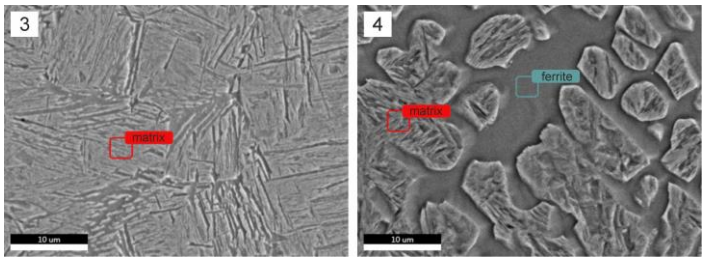

Figure 6 Microstructure of weld metal of weld 3 and 4 with assigned regions investigated by EDS, scale 10 µm

Table 3 EDS analysis of base metal and weld metal matrix

Element	Base metal	Weld			
		1	2	3	4
Si (wt%)	0.24	0.40	0.42	0.32	0.47
Al (wt%)	0.07	1.34	1.61	0.77	1.83

4. DISCUSSION

The microstructure of the weld metal of 22MnB5 should be fully martensitic at cooling faster than 16 °C·s^{-1} [11]. In our setup, orderly higher cooling rates can be expected at least for the welds made with the focused beam. Based on the model tuned for a 1.5 mm thin sheet of low-alloyed steel to reach the cross-section of weld 1, the cooling rate is about 550 °C·s^{-1}. However, the bainitic-martensitic microstructure was identified with EBSD in the welds of sheets both with and without the coating. The changes in cooling rate induced by different heat inputs play a minor role compared to the changes in the chemical composition of weld metal.

When welding the coated sheet, the coating solutes and the weld metal enriches with Al and Si. Both the Si and especially the Al are strong ferrite stabilizers moving the ferrite transformation to much shorter times in the continuous cooling transformation (CCT) diagram [12], thus promoting the formation of ferrite at higher cooling rates. Concerning the low heat input, characteristic of focused beam welding, the weld metal homogenization is very limited, and only local bands of ferrite appear in the regions with increased content of Al and Si. The ferritic bands are very rare and rather close to the fusion line in weld 1. In weld 4, made with beam oscillation, the bands are larger which corresponds to the higher volume of dissolved coating and much faster cooling rate resulting from the spot speed of up to 600 mm·s^{-1}.

The higher heat input accompanying the welds made with the defocused beam allows a higher level of homogenization resulting in a little average increase in Si and Al throughout the weld metal towards the base metal. Therefore, only a small shift of the ferrite start curve in the CCT diagram can be predicted and may not affect the weld metal microstructure at sufficiently high cooling rates (weld 3). The shift increases with an increasing portion of the dissolved coating. Therefore, the ferritic islands are interspersed throughout the homogenized weld metal of the weld 2 having the coating content double compared to the weld 3.

5. CONCLUSION

The effect of welding parameters on the macrostructure and weld metal microstructure of 22MnB5+AlSi laser welds was demonstrated. The presence of Al-Si coating promotes the formation of ferrite in the weld metal. The distribution and content of ferrite depend on the heat input and the volume of the dissolved coating which change with any modification of welding parameters or technology. Thus, predicting the ferrite distribution is a

very challenging task. Particularly in laser welding with beam oscillation, the large ferrite bands might weaken the weld joint. Further research will focus on the effect of ferrite distribution on weld mechanical properties.

ACKNOWLEDGEMENTS

This work was supported by the Technology Agency of the Czech Republic [grant number FW01010293]; and the Academy of Sciences of the Czech Republic [Strategy AV21 "Light in the service of society"]. The institutional support RVO:68081731 is gratefully acknowledged.

REFERENCES

[1] PARAREDA, S., CASELLAS, D., FRÓMETA, D., MARTÍNEZ, M., LARA, A., BARRERO, A., PUJANTE, J. Fatigue resistance of press hardened 22MnB5 steels. *International Journal of Fatigue*. 2020, vol. 130, p. 105262. Available from: https://doi.org/10.1016/j.ijfatigue.2019.105262

[2] GU, Z., YU, S., HAN, L., LI, X., XU, H. Influence of welding speed on microstructures and properties of ultra-high strength steel sheets in laser welding. *ISIJ International*. 2012, vol. 52, pp. 483–487. Available from: https://doi.org/10.2355/isijinternational.52.483

[3] JIA, J., YANG, S.L., NI, W.Y., BAI, J.Y. Microstructure and mechanical properties of fiber laser welded joints of ultrahigh-strength steel 22MnB5 and dual-phase steels. *Journal of Materials Research*. 2014, vol. 29, pp. 2565–2575. Available from: https://doi.org/10.1557/jmr.2014.273

[4] GRAUER, S.J., CARON, E.J.F.R. CHESTER, N.L., WELLS, M.A., DAUN, K.J. Investigation of melting in the Al–Si coating of a boron steel sheet by differential scanning calorimetry. *Journal of Materials Processing Technology*. 2015, vol. 216, pp. 89–94. Available from: https://doi.org/10.1016/j.jmatprotec.2014.09.001

[5] KÜGLER, H., MITTELSTÄDT, C., VOLLERTSEN, F. Influence of joint configuration on the strength of laser welded presshardened steel. *Physics Procedia*. 2016, vol. 83, pp. 373–382. Available from: https://doi.org/10.1016/j.phpro.2016.08.039

[6] SUN, Q., DI, H.S., WANG, X.N., CHEN, X.M., QI, X.N., LI, J.P. A Study on Microstructure and Properties of PHS Fiber Laser Welded Joints Obtained in Air Atmospheres. *Materials*. 2018, vol. 11, p. 1135. Available from: https://doi.org/10.3390/ma11071135

[7] ŠEBESTOVÁ, H., HORNÍK, P., MIKMEKOVÁ, Š., MRŇA, L., DOLEŽAL, P., NOVOTNÝ, J. Microstructural characterization of laser weld of hot-stamped Al-Si coated 22MnB5 and modification of weld properties by hybrid welding. *Materials*. 2021, vol. 14, issue 14, p. 3943. Available from: https://doi.org/10.3390/ma14143943

[8] THIEL, C., HESS, A., WEBWER, R., GRAF T. Stabilization of laser welding processes by means of beam oscillation. In: *Proceeding SPIE: Laser Sources and Applications*. Brussels: SPIE, 2012, vol. 8433, p. 84330V. Available from: https://doi.org/10.1117/12.922403

[9] FRANCO, D., OLIVIERA, J.P., SANTOS, T.G., MIRANDA, R. M. Analysis of copper sheets welded by fiber laser with beam oscillation. *Optics and Laser Technology*. 2021, vol. 133, p. 106563. Available from: https://doi.org/10.1016/J.OPTLASTEC.2020.106563

[10] HORNÍK, P., ŠEBESTOVÁ, H., NOVOTNÝ, J., MRŇA, L. Laser beam oscillation strategy for weld geometry variation. *Journal of Manufacturing Processes*. 2022, vol. 84, pp. 216–222. Available from: https://doi.org/10.1016/J.JMAPRO.2022.10.016.

[11] NIKRAVESH, M., NADERI, M., AKBARI, G. H., BLECK, W. Bleck. Phase transformations in a simulated hot stamping process of the boron bearing steel. *Materials and Design*. 2015, vol. 84, pp. 18–24. Available from: https://doi.org/10.1016/j.matdes.2015.06.108

[12] GOMEZ, M., GARCIA, C. I., HAEZEBROUCK, D. M., DEARDO, A. J. Design of composition in (Al/Si)-alloyed TRIP steels. *ISIJ International*. 2009, vol. 49, no. 2, pp. 302–311. Available from: https://doi.org/10.2355/isijinternational.49.302